Simple and fast design of folic acid-based carbon dots as theranostic agent and its drug release aspect

by Mochamad Zakki Fahmi

Submission date: 01-Sep-2021 08:59PM (UTC+0800)
Submission ID: 1639432665
File name: as_theranostic_agent_and_its_drug_release_aspect_compressed.pdf (725.3K)
Word count: 7921
Character count: 41643

Materials Chemistry and Physics 267 (2021) 124596

Contents lists available at ScienceDirect

Materials Chemistry and Physics

journal homepage: www.elsevier.com/locate/matchemphys

Simple and fast design of folic acid-based carbon dots as theranostic agent and its drug release aspect

Mochamad Z. Fahmi [a,b,*], Novia F. Sholihah [a], Aswandi Wibrianto [a], Satya C.W. Sakti [a,b], Fakhri Firdaus [a], Jia-yaw Chang [c]

[a] Department of Chemistry, Universitas Airlangga, Surabaya, 60115, Indonesia
[b] Supramodification Nano-Micro Engineering Research Group, Universitas Airlangga, Surabaya, 60115, Indonesia
[c] Department of Chemical Engineering, Department of Chemical Engineering, National Taiwan University of Science and Technology, 43, Section 4, Keelung Road, Taipei, Taiwan, China

HIGHLIGHTS

- Synthesis of CDs from folic acid as Doxorubicin Delivery through simple steps.
- Comparison FACDs properties prepared from furnace and microwave assisted methods.
- The release of Doxorubicin follows Korsmeyer-Peppas kinetics model and accelerate on acid condition.
- All FACDS perform low cytotoxicity and can work on delivering the drug well.

GRAPHICAL ABSTRACT

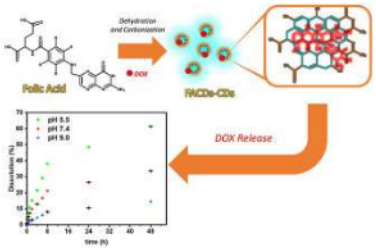

ARTICLE INFO

Keywords:
Folic acid
Carbon dots
Bioimaging
Kinetic release
Flow cytometry

ABSTRACT

The usage of folic acid as source carbon dots is an excellent way to promote its efficient and specific target to folate receptor expressed cells, even the most methods serve on the complicated procedure. This research was conducted by synthesizing folic acid-based carbon dots (FACDs) through furnace and microwave-assisted methods to offer a simple and effective process. Thermal treatment belongs to the methods that allow both dehydration and carbonization of folic acid to produce graphene oxide-like structure carbon dots. The successful synthesis process was convinced with some characterization data, like diameter size of FACDs was below than 6 nm sizes and photoluminescence at emission 481 nm. Further FTIR, Raman, and XPS analysis demonstrated potency formation of graphene oxide-like structure on CDs within a non-polar feature. In vitro assessment through CCK-8, flow cytometry, and confocal microscopy revealed that all of the prepared FACDs perform low-toxicity and work well on HeLa cancer staining by folate receptor-mediated endocytosis into the cell cytoplasm. On the good agreement with diagnostic capability on the cell, FACDs produced by both methods also perform excellent therapeutic capability on doxorubicin delivery with its kinetical release follow the Korsmeyer-Peppas model. All the findings confirm that the methods were excellent ways to perform good FACDs as theranostic agents for biological applications.

* Corresponding author. Department of Chemistry, Universitas Airlangga, Surabaya, 60115, Indonesia.
E-mail addresses: m.zakki.fahmi@fst.unair.ac.id (M.Z. Fahmi), novia.faridatus.olihah-2015@fst.unair.ac.id (N.F. Sholihah), aswandi.wibrianto-2016@fst.unair.ac.id (A. Wibrianto), satya.sakti@fst.unair.ac.id (S.C.W. Sakti), fakhri.firdaus-2016@fst.unair.ac.id (F. Firdaus), jychang@mail.ntust.edu.tw (J.-y. Chang).

https://doi.org/10.1016/j.matchemphys.2021.124596
Received 5 January 2021; Received in revised form 23 March 2021; Accepted 3 April 2021
Available online 19 April 2021
0254-0584/

Abbreviation

Carbon dots	(CDs)
Quantum yield	(QY)
Furnace-assisted carbon dots	(FACDs-P)
Microwave-assisted carbon dots	(FACDs-M)
Folic acid	(FA)
Ultra violet-visible	(UV–Vis)
X-ray diffraction	(XRD)
X-ray photoelectron spectroscopy	(XPS)
Photoluminescence	(PL)
Fourier Transform Infra-red	(FTIR)
Atomic spectrum force microscope	(AFM)
Cell counting kit 8	(CCK-8)
Confocal laser scanning microscope	(CLSM)
Doxorubicin	(DOX)
Dimethyl sulfoxide	(DMSO)
Sodium hydroxide	(NaOH)
Ethanol	(C_2H_5OH)
Dulbecco's Modified Eagle Medium	(DMEM)
Phosphate-buffered saline	(PBS)
cytotoxic concentration	(CC_{50})
Rhodamine 6G	(R6G)
Propidium iodide	(PI)

1. Introduction

In biomarker application of the tumor cell, the constraints of effectiveness, complicated design, scarce price, and selectivity to target cells are still important aspects that need to be investigated even further. These issues drive several studies to develop nanomaterial attributed with targeting to sites overexpressing on cancer cell, such as folate [1,2], CD44 [3], integrin [4], transferrin [5], glycoprotein-based [6], growth factor-based receptors [7], to promote effectiveness on its clinical purpose. Compared with the other existing targeting agent, folic acid was a commercial compound that facile founded on the membrane of some cancer cells such as in the cervix, brain, eyes, liver, and lungs [8]. Moreover, folic acid (FA) is a promising ligand due to its high biocompatibility and great affinity ($K_d \sim 10^{-10}$ M) in both hydrophilic and hydrophobic solutions [9,10]. These fascinating properties made FA becomes a promising agent as a detector of particular folate receptors in order to recognize clearly cancer cells location [11]. Recently, many researchers have developed nanoparticles conjugated with folic acid for fluorescence optimization higher selectivity in targeting of cancer cells [12,13]. However, recent studies on folic acid conjugated nanoparticles still emerge several obstacles to be solved, like the multi-step synthesis method [14], a large number of reagents used, the unpromising optical properties [15], and hardly binding to a specific region of targeting cancer cells [16].

Among several kinds of nanomaterial performed for cancer therapy, carbon dots (CDs) have been developed massively regarding optical and non-toxic properties associated with, that profoundly required as biomarker agent on biological applications [17]. Even commonly made from graphene or graphene oxide derivates, some researches also proved successful synthesis of CDs from organic small compounds and natural products [18]. Moreover, several studies have found interesting ideas on using folic acid as a precursor in carbon dot synthesis and its utilization as a biomarker of cancer cells [15]. The methods in folic acid carbon dot synthesis are generally classified into two ways, namely: top-down and bottom-up methods [19]. The top-down method is a physical synthesis method including laser arc discharge method [20], ablation method [21], and plasma treatment [22], while the bottom-up method is a chemical synthesis method that includes electrochemical, hydrothermal [23], pyrolysis [24], and microwave-assisted methods [25]. Various kinds of research on the synthesis of CDs have been carried out with different methods. Based on the previous study, abundant folic acid-based carbon dots (FACDs) synthesized by the hydrothermal method showed complicated treatment for the fabrications process, identified by further sonication, centrifugation, and precipitation after heated in the hydrothermal state [26]. Besides, the microwave method is a method that is carried out by heating using microwaves. The resulting microwaves can simplify and speed up the synthesis process. Another technique that involves a heating process is furnace-assisted. The method is classified as a simple synthesis process owing to its oxygen-free heating principle [27]. As pursued in previous studies, a simple approach for the formation of fluorescent CDs that target cancer cells by folic acid as the carbon precursor in CDs fabrication has been conducted [15,28]. The CDs were synthesized in a simple single-step process without conjugating folic acid with the prepared CDs. However, the synthesized CDs still exhibit a low QY value.

Table 1
Composition of the folic acid based CDs.

Sample ID	Method	Time		
		FA	min	h
FACDs-P1	Furnace-assisted	0.10	2	–
FACDs-P2		0.10	–	2
FACDs-M1	Microwave-assisted	0.10	2	–
FACDs-M2		0.10	–	2

Therefore, it is necessary to perform simple synthesis (one-pot) and excellent photoluminescence effect and accurately targeted cell delivery drugs in biomedical applications. This study was applied to compare the FACDs synthesis process that has never been explored before, with a furnace-assisted and microwave-assisted approach. A favorable FACDs were examined by optical and physical properties, equipped by UV–Vis, Photoluminescence, Fourier transform infrared, Raman, X-ray photoelectron Spectrophotometer, X-ray diffractometer, and Atomic force microscope. CCK-8 assay was utilized to evaluate the toxicity of CDs and using CLSM test to capture the FACDs ability as a staining agent for the HeLa cancer cell supported by kinetic release study.

2. Experimental

2.1. Materials

Folic acid (FA, ≤97%), sodium hydroxide (NaOH), and methanol (CH_3OH, 96%) were purchased from Merck (Germany). Dimethyl sulfoxide (DMSO, 99.7%) were purchased from Sigma-Aldrich (Germany). Ethanol (C_2H_5OH, 94–96%) was purchased from J.T. Baker (Malaysia). Hydrogen chloride (HCl, 37%) was purchased from Merck (Germany). Cell Counting Kit-8 (CCK-8) cytotoxicity kit was purchased from MedChemExpress (USA). DOX was purchased from Tokyo Chemical Industry Co., Ltd. (Tokyo, Japan). These chemicals were used directly in the research and without any further purifications.

2.2. Synthesis of folic acid carbon dots by furnace and microwave-assisted

The CDs were obtained by heating folic acid (10.0 mg) following the composition in Table 1, respectively. For the furnace-assisted method, each sample was calcined at 270 °C on the isolated reactor. For the microwave-assisted method, the folic acid was dissolved in 300 μL NaOH 0.1 M and (following in Table 1) settled into a microwave reaction system with 600-W power and high temperature. For all of the

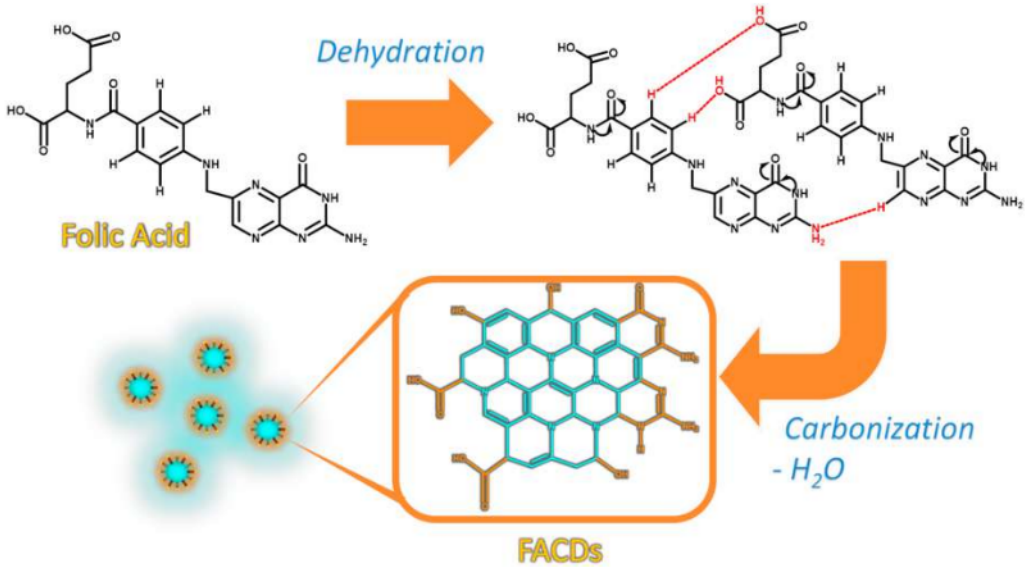

Scheme 1. Schematic mechanism for formation of FACDs on furnace (FACDs-P1 and FACDs-P2) and microwave (FACDs-M1 and FACDs-M2) assisted methods.

samples, after the samples were cooled down to room temperature naturally, the dark brown CDs were obtained by collect stacked precipitate on the bottom of the reactor. To prepare its colloidal solution, the FACDs with adjusted concentration are first prepared by dissolving on NaOH solution (0.1 M) and set the pH on neutral value. The synthesized solution was further dialyzed on the molecular weight cut-off membrane (MWCO) of 1000 Da to specify the size distribution of the CDs and to exempt unwanted particles [29].

2.3. Preparation of DOX-loaded folic acid-based carbon dots (FACDS-DOX), drug release, and kinetic evaluation

To prepare DOX-loaded folic acid-based carbon dots (FACDs-DOX), DOX solution (10 mL; 1000 mg/mL) was combined into FACDs and rapidly stirred at 30 °C (24 h). After that, the loading FACDs-DOX was dialyzed on deionized water for 2 h using a membrane (MWCO 1000 Da; Cellu Sep H1, Orange Scientifique, Belgium) to remove the free DOX from the FACDs mixture. The DOX concentration in FACDs was determined by measuring all samples absorption at 485 nm and matching it to a standard calibration curve. The loading amount and efficiency of DOX are calculated based on equations (1) and (2) as follows:

$$Loading \cdot Amount \cdot (\%) \cdot = \cdot \frac{m_{DOX}}{m_{FACDs}} \times 100 \quad (1)$$

$$Loading \cdot Efficiency \cdot (\%) \cdot = \cdot \frac{m_{DOX}}{m_{FACDs-DOX}} \times 100 \quad (2)$$

Determination of the exact concentration of released DOX was acquired with these following equations:

$$C_t \cdot = \cdot C_m + \frac{v}{V} \sum_{0}^{t-1} C_m \quad (3)$$

where C_t (ppm) and C_m are the exact and the measured concentration at time t (s), v and V are the taken volume and total volume of the DI water (mL).

The DOX release mechanism was fitted by analyzing its dissolution outline with two models of kinetic study, particularly Higuchi, and Korsmeyer-Peppas, that offer as Equation (4) – (5), respectively.

$$F_H = K_H . t^{1/2} \quad (4)$$

where F_H is the released DOX fraction in time t and K_H is the constant of Higuchi release ($s^{-1/2}$).

$$\frac{m_t}{m_\infty} \cdot = \cdot K_{KP} \cdot t^n \quad (5)$$

where Mt and M_∞ are the amount of DOX released at time t and ∞, respectively, K_{KP} is the costant of Korsmeyer-Peppas release and n is DOX release exponent. Fickian diffusion is signified by n value ($n \leq 0.5$), non-Fickian diffusion ($0.5 < n < 1$) and release kinetic time independence (i.e. zero-order model) is implied if $n \geq 1$.

2.4. Viability cells assessment

The cytotoxicity test of FACDs was detected in HeLa cell lines by Cell Counting Kit-8 (CCK-8) assay (MedChemExpress, New Jersey, USA). HeLa cell lines were first cultured at a 96-well plate with 2.5×10^4 cells per well containing Dulbecco's Modified Eagle Medium (DMEM) and incubated for 24 h. Then, phosphate-buffered saline (PBS) was added to wash the cells. The cells were further incubated on 100 μL of DMEM with varied concentrations of FACDs (10 μL) and varied times. Once the adjusted time was reached, the cell was continued by adding one mL of CCK-8 reagent (500 mg/mL) and incubated for 4 h. The absorbance of formazan on each plate correlated with the living cell was analyzed by using a microplate reader at 450 nm. The cytotoxicity effects of doped-carbon dots were assessed at half the cytotoxic concentration (CC_{50}) and fixed using Origin 2018 software.

2.5. CLSM imaging assessment

For preparation, HeLa cells were cultured at 96 well-plate containing 2 mL Dulbecco's Modified Eagle Medium (DMEM) and incubated for 24 h. Each FACDs (400 μL) was further added and incubated for 1 h. Then, the cells were rinsed by PBS three times and then fixed with 70% alcohol for about 10 min. Fluorescence images of FACDs in HeLa cells were captured from cells for immersion of 63 × 1.32 NA oil by confocal TCS SP2 (Leica Microsystems, USA) equipped with inverted microscopy and inline Ar (488 nm) and He–Ne (503–680 nm and 588 nm) laser.

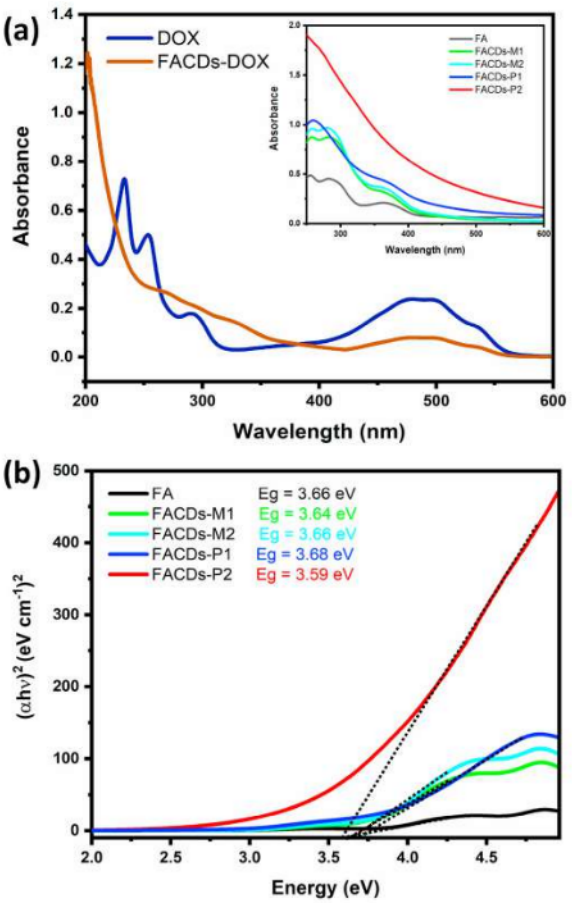

Fig. 1. UV–Vis spectra of (a) FACDs using microwave and furnace-assisted methods, Doxorubicin (DOX) (dark blue), and loading FACDs-DOX (brown). (b) Tauc plot of FACDs by microwave and furnace-assisted methods. (For interpretation of the references to colour in this figure legend, the reader is referred to the Web version of this article.)

2.6. Flow cytometry assessment

For 24 h, approximately 3 × 105 HeLa cells were cultured in a cell flask T75 with a 5 mL medium. A 5 mL fresh medium, later on, replaced the last medium containing various concentrations of samples, supported by PBS-treated cells as a control. The treated cells were rinsed with PBS, trypsinized, centrifuged, and suspended in the binding buffer after 1 h incubation. The cells were then stained with a 5 μL Annexin V-FITC for 15 min, washed with binding buffer, and stained with a 10 μL propidium iodide. The samples were analyzed on a Guava easyCyte Flow Cytometer supplied by an argon laser (488 nm).

2.7. Other characterizations

The synthesized products were characterized by several instruments. Fourier Transform Infra-red (FTIR) spectra were measured by Infrared (IR) Tracer-100 (Shimadzu, Japan). Ultraviolet–visible (UV–Vis) spectra were exhibited by using spectrophotometer UV–Vis Shimadzu 1800 (Shimadzu, Japan). Zeta Potential Values of FACDs were determined by PALS Zeta Potential Analyzer (Brookhaven, USA). The photoluminescence of doping carbon dots was collected by LS 55 fluorescence spectrometer (Shimadzu, Japan). The PL of FACDs was determined comparatively by remarking rhodamine 6G (R6G, QY (95%)), the %QY of FACDs were determined by this following equation:

$$QY = QY_{R6G}\ (I_{CDs}/I_{R6G})\ (A_{CDs}/A_{R6G})\ (\eta_{water}/\eta_{ethanol})^2 \quad (6)$$

where I, A, and η are the integral PL intensity, UV absorbance, and the optical density and reflective index of the solvent, respectively. Atomic Force Microscopy (AFM) images were acquired by Nanoscan type AFM (Bruker, Germany). X-ray photoelectron spectroscopy (XPS) spectra of FACDs were obtained from X-ray photoelectron spectrometer Ulvac-PHI supported by Al-Kα X-ray source and a monochromator. XRD patterns were investigated by Philips source X-ray diffractometer set by Cu $K\alpha_1$ line (λ = 1.54 Å).

2.8. Statistical analysis

The 50% cytotoxic concentration on cell viability (CC_{50}), was determined by the dose-response model (nonlinear fitting) of Origin software (version 8.0724, OriginLab Inc., Northampton, MA). All data were acquired in triplicate, with sample *t*-test on some data.

3. Results and discussion

The FACDs were synthesized by merely handling folic acid through a furnace and microwave-assisted method (Scheme 1). Even mechanism synthesis of CDs does not fix yet, dehydration and carbonization processes occur theoretically during thermal treatment on both methods, respectively [30]. Then, this condition will initiate rearrangement of the folic acid structure as strong as its combination to form a graphene oxide-like structure. Nevertheless, this reassembling process was initiated by hydrogen bonds occurring between folic acid itself (as displayed on Scheme 1) [31]. According to equation (2), the drug loading capacity of DOX on FACDs was calculated at nearly 62%. The high loading capacity could be related to the electrostatic interaction (non-covalent bonding) between DOX and FACDs [32]. The conjugate may become more biocompatible by surface modification using a linker, i.e. bovine serum albumin (BSA) [13]. Furthermore, the formation of FACDs-DOX Graphene oxide (GO) structure will be obtained in CDs core due to further carbonization which was confirmed by performing luminescence of FACDs under UV light.

The absorption pattern was shown in FACDs-M1 and FACDs-M2 in Fig. 1a resulted in two absorption peaks, namely at 259 nm and 280 nm, respectively. The absorption peak of 259 nm indicates the occurrence of an electron transition π→π* and the absorption peak of 280 nm signifies an electron transition of n→π* of moiety on the FACDs [33,34]. The FACDs-M1 and FACDs-M2 have almost the same wavelength, namely in the 256–280 nm range. Nevertheless, the FACDs-M2 delivered greater absorbance compared to the FACDs-M1, due to the carbonization process using the microwave method in FACDs-M2 lasts longer, so the process of synthesizing carbon dots is better when compared to FACDs-M1, whereas, in the carbon dots samples FACDs-P1 and FACDs-P2, the absorption pattern formed in the furnace-assisted method had one absorption peak at 259 nm which demonstrates the electron transition π→π* (core). In the graph of the furnace-assisted method on FACDs-P2, the carbon dots structure in surface state form did not reveal its absorption peak. However, the peak of the surface state was still there, it is just that when the UV–Vis test was carried out, the peak was unreadable owing to the carbonization process formed on carbon dots was too high. Further investigation by analyzing Doxorubicin (DOX) and loading FACDs-DOX was shown a specific region at 485 nm which symbolized a presence of DOX in loading FACDs-DOX [35,36]. The bandgap of FACDs, represented by Fig. 1b, indicated all samples are in similar sizes [37].

The image of all FACDs in Fig. 2a–f were light yellow in daylight and exhibited strong blue luminescence under UV light [38]. Folic acid and

carbon dots excitation were analyzed at 320 nm and an emission wavelength range from 340 to 400 nm. FACDs-M1 and FACDs-M2 in Fig. 2a and b displayed emission at 447 nm and 487 nm, respectively, whereas FACDs-P1 and FACDs-P2 Fig. 2c and d showed emission wavelengths of 434 nm and 481 nm, respectively. Pure folic acid, as shown in Fig. 2e showed emissions at 398.5 nm. From these data, folic acid has a low emission intensity, nevertheless, carbon dots exhibit higher emissions due to the formation of conjugated π-domains (carbon core) of carbon dots structure [39,40]. Further investigation to overcome the quantum yield (QY) of each FACDs was analyzed by LS 55 fluorescence spectrometer (Shimadzu, Japan) [41,42]. Furthermore, using R6G as a reference (QY = 95%% in 0.1 M ethanol, $\lambda_{ex} = 320$ nm), the quantum yield (QY) of folic acid carbon dots in samples FACDs-P1, FACDs-P2, FACDs-M1 and FACDs-M2 contributed 55.7%, 3.6%, 9.5%, 2.8%, respectively. The QY data form obtained FACDs are comparable with previous studies, which is exhibit excellent optical properties of CDs (Table S1). FTIR spectra of FACDs, as displayed in Fig. 3, presented the appearance of varied functional groups. Folic acid (FA) had a broad absorption at 3358.06 cm^{-1} and 2918.29 cm^{-1} which symbolized a stretching vibration of O–H and C–H. The 1652.99 cm^{-1} corresponded to the presence of a carbonyl group (C═O) of carboxylic acid. stretching (C═C) of benzene was indicated at 1558.14 cm^{-1}, and stretching (C–N) at wave number 1338.59 cm^{-1} [43]. FACDs-P1 has a similar functional group, including O–H stretching, CH stretching, C═O carboxylic acid, C═C benzene, and C–N at 3365.78 cm^{-1}, 2891.29 cm^{-1}, 1705.07 cm^{-1}, 1429.25 cm^{-1}, 1093.63 cm^{-1}, respectively [44]. Moreover, FACDs-P2 demonstrated O–H stretching, C–H stretching, C═O carboxylic acid, C═C benzene, and C–N at 3450.65 cm^{-1}, 2891.29 cm^{-1}, 1705.07 cm^{-1}, 1591.27 cm^{-1}, and 1226.72 cm^{-1}, respectively. In addition, FACDs-M1 showed stretching vibration of O–H, C–H, C═O (carboxylic acid), C═C benzene, and C–N particularly at 3381.21 cm^{-1}, 2918.29 cm^{-1}, 1658.78 cm^{-1}, 1598.98 cm^{-1}, 1409.96 cm^{-1}, 1145.71 cm^{-1} [25], whereas FACDs-M2 also emitted O–H stretching functional groups, C═O carboxylic acid, C═C benzene, and C–N at 3246.19 cm^{-1}, 1656.85 cm^{-1}, 1419.60 cm^{-1}, 1143.78 cm^{-1}, respectively [45].

Further 2D morphology study of CDs is performed by AFM demonstrating the distribution and particle sizes of FACDs in Fig. S1. Further improvement on AFM data by using ImageJ software to adjust size

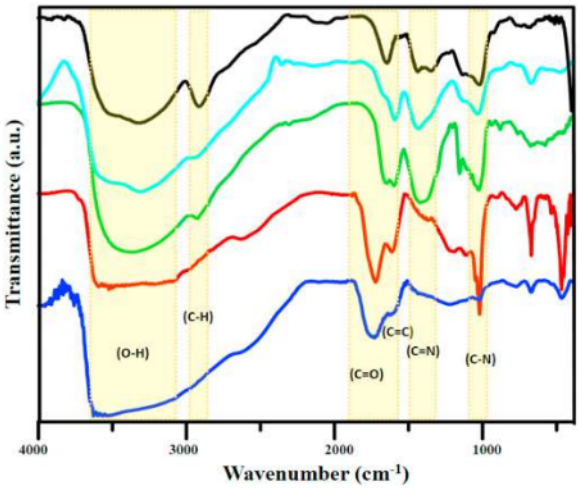

Fig. 3. Infra-Red spectra of folic acid (FA) and carbon dots FACDs-M1 (green); FACDs-M2 (aqua); FACDs-P1 (blue); FACDs-P2 (red) by microwave-assisted and furnace-assisted methods. (For interpretation of the references to colour in this figure legend, the reader is referred to the Web version of this article.)

distribution of the obtained CDs, where all FACDs, as shown in Fig. S1a, FACDs exhibited average diameter sizes under 6 nm. The height of the particles also distributed homogenously displayed in Figs. S1b and c, which are classified as carbon dots owing to the diameter size below 10 nm with a mostly spherical shape [46]. FACDs-P and FACDs-M in Fig. 4a and e carbon dots were investigated even further using X-ray photoelectron spectroscopy (XPS) to acquire the existence of the atom, including, carbon (C1s), oxygen (O1s), and nitrogen (N1s). The XPS C1s spectrum of FACDs was shown in Fig. 4b displayed the presence of carbon signals at 284.5 (i), 285.7 (ii), and 288.6 eV (iii), respectively, corresponding to the existence of C═C (benzene), C–N/C–O, and a carboxyl group. Besides, three peaks in the C1s region were yielded from

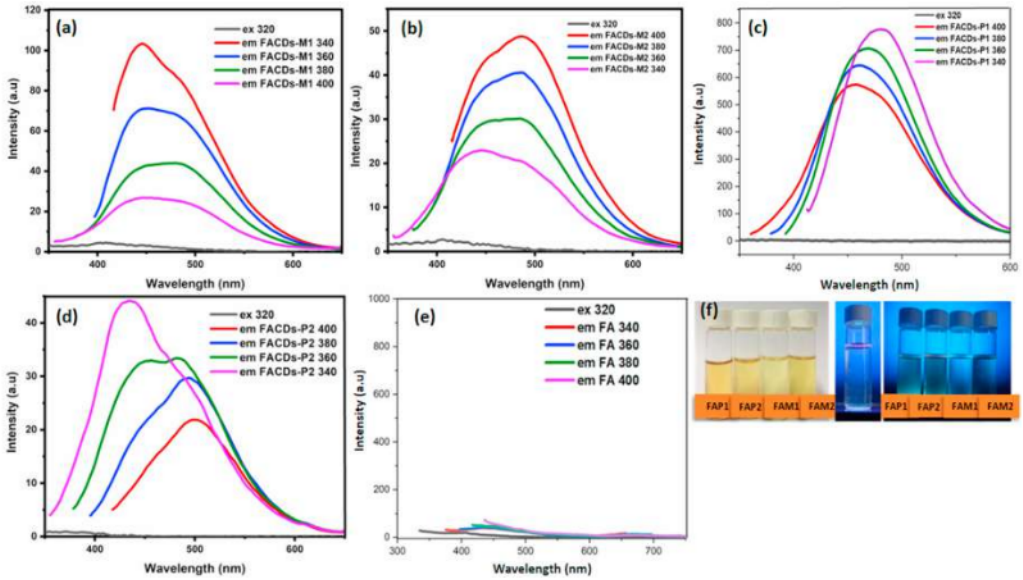

Fig. 2. PL Spectra of (a) FACDs-M1, (b) FACDs-M2, (c) FACDs-P1, (d) FACDs-P2, (e) FA, and (f) Photographs of doped CDs under daylight and UV-light prepared by furnace and microwave-assisted methods.

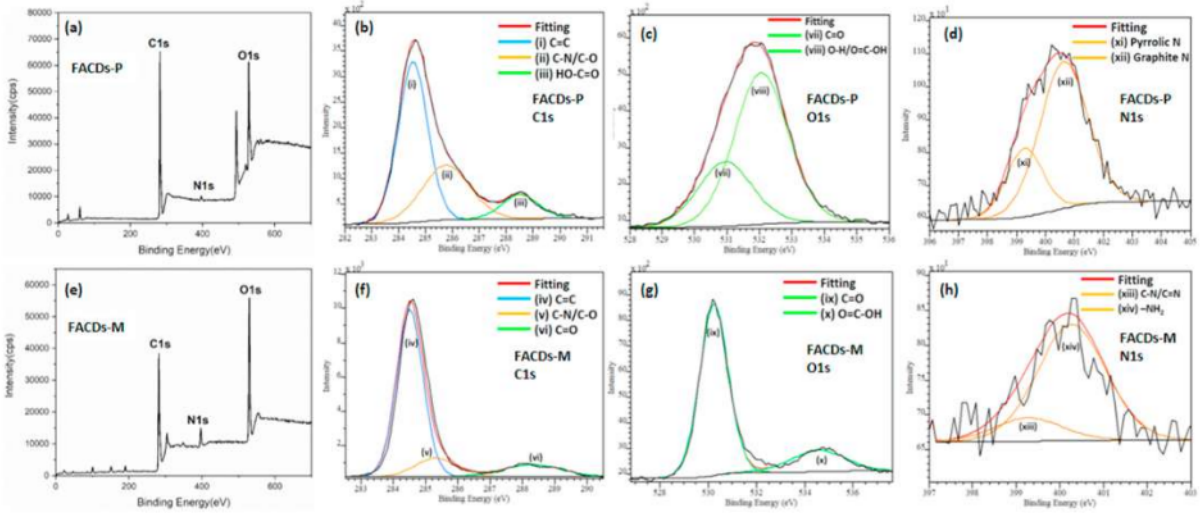

Fig. 4. XPS spectra of FACDs-P (a) full scan, (b) C1s, (c) O1s, and (d) N1s by microwave-assisted method. (e) Full survey scan of FACD-M, (f) C1s, (g) O1s, and (h) N1s regions using furnace-assisted method.

FACDs-M in Fig. 4f at 284.6 (iv), 285.3 (v), and 288.3 eV (vi) corresponding to C═C, and C–N, and C═O, respectively [47,48]. The O1s region of FACDs-P in Fig. 4c has two peaks at 530.9 (vii) and 532.1 eV (viii), symbolizing C═O and C–OH/O═C–OH, respectively [49]. In Fig. 4g, The O1s spectra of FACDs-M presented the existence of C═O and O═C–OH at 530.2 (ix) and 534.2 eV (x), respectively. The N1s spectrum of the FACDs-P is represented by two peaks, at 399.4 (xi) and 400.7 eV (xii), associated with pyrrolic N and graphite N, respectively [50]. Moreover, the N1s spectrum of the FACDs-M exhibited C–N/C═N and –NH_2 peaks at 399.3 (xiii) and 400.4 eV (xiv), respectively [51]. The predominance of hydroyl and carbonyl groups over others functional groups also well-revealed by the XPS data, which XPS intensity of oxygen element was higher than other elements, exclude carbon element. This condition support the stability of the CDs upon polar solvents. Zeta potential values supported the XPS data, which FACDs-P1; FACDs-P2; FACDs-M1; FACDs-M2 show zeta potential on quite similar values about −19,28; −21,21; −20,60; −21,82, respectively, referring hydroxyl and carbonyl groups majorly exists on the CDs. Further Raman spectra of carbon dots were exhibited in Fig. 5a, the FACDs-P1 spectrum showed the D and G band peaks at 1329.79 cm^{-1}, 1519.39 cm^{-1}, FACDs-P2 displayed the D and G bands at 1335.19 cm^{-1}, 1566.72 cm^{-1}, respectively [52,53]. Additionally, the FACDs-M1 spectra presented D and G bands at 1229.25 cm^{-1} and 1437.30 cm^{-1}. Moreover, the D and G band peaks of the FACDs-M2 are shown at 1313.55 cm^{-1} and 1556.23

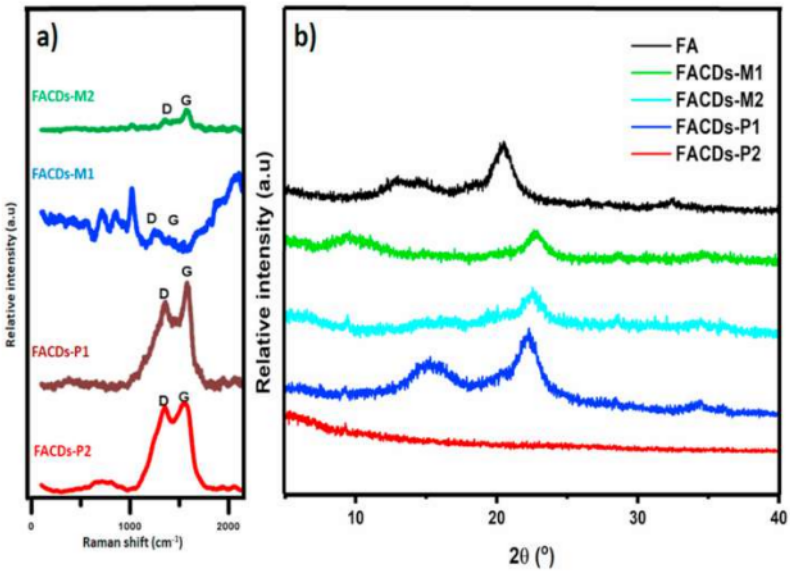

Fig. 5. (a) Raman scattering spectra of FACDs-M2 (green), FACDs-M1 (blue), FACDs-P2 (dark brown), and FACDs-P1 (red). (b) XRD Diffractogram of folic acid and carbon dots FACDs-M1; FACDs-M2; FACDs-P1; FACDs-P2. (For interpretation of the references to colour in this figure legend, the reader is referred to the Web version of this article.)

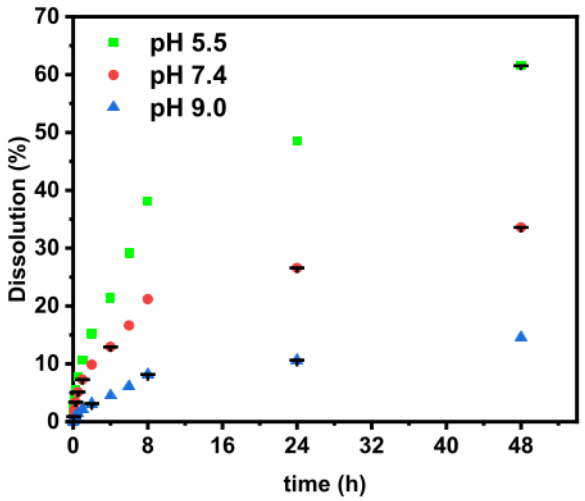

Fig. 6. The DOX dissolution rate in loading FACDs-DOX at varied pH condition. The data mesure as average of three replications.

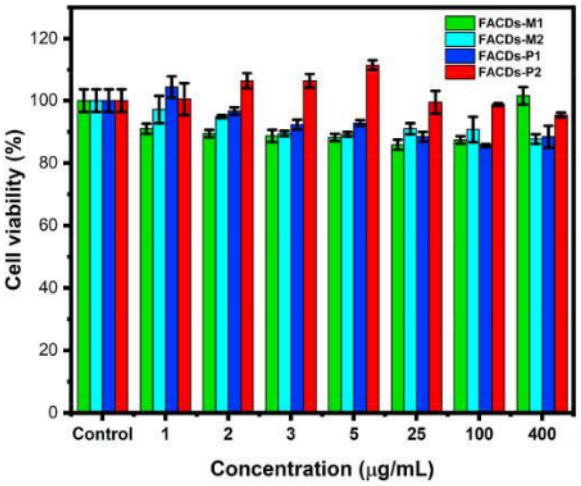

Fig. 7. Cell viability histogram of HeLa cancer cells after 24 h incubation by varying concentrations of furnace-assisted method FACDs-P and microwave-assisted method FACDs-M. All data displayed as mean ± SD with n = 3.

cm^{-1}, respectively [54]. The D band is related to the deficiency of the carbon structure that reverses structural defects and is associated with the part of the sp^3 conformation obtained due to the amorphous formation of graphite within the process of oxidation whereas the G band comes from vibrations in the sp^2 carbon atomic plane. The smaller the D and G band (I_D/I_G) intensity ratio, the better the formation of CDs. This is observed by the reduced sp^3 conformation content on carbon, higher levels of graphitization, and a more uniform surface state [55]. Among the FACDs, the intensity ratio of D and G band (I_D/I_G) particularly from lowest to higher are FACDs-M2<FACDs-P2 <FACDs-M1 <FACDs-P1, respectively. The D and G band (I_D/I_G) intensity ratios are very susceptible to structural changes in the carbon matrix which can be influenced by several factors such as substrate. defects, and doping [56]. The diffractogram pattern of FACDs-P1, FACDs-P2, FACDs-M1, FACDs-M2 in Fig. 5b revealed amorphous solid. The synthesis of carbon dots utilizing either furnace or microwave-assisted methods results in the process of dehydration from the surface of the solid, leaving a lower amorphous or carbonate anhydrous material. Furthermore, the pattern analysis results are compared with JCPDS 01–0646 database, which corresponding to graphene-like structure [57,58]. Further investigation of FACDs-P1, FACDs-P2, FACDs-M1, FACDs-M2 resulted in d-spacing of 0.6453 nm, 0.1876 nm, 0.76567 nm, and 0.7356 nm, respectively.

3.1. In vitro drug release activities

Incorporation of DOX upon FACDs was served through van der Waals and π-π attraction between polybenzene performed on both FACDs and DOX. This attraction considered more benefit to give facile releasing of the drug on the target. However, release pattern of DOX that just physical binding with FACDs became critical issue. The DOX release over time was examined and the results are displayed in Fig. 6. The dissolution of DOX of loading FACDs-DOX was investigated at varied pH buffers (pH = 5.5, 7.4, and 9.0). The fastest release of DOX was attained at pH 5 (approximately 65.7%) of the loaded DOX was released toward the buffer within 48 h. The dissolution percentage of loading DOX decreases with increasing pH in buffer solution (pH 7.4 and 9.0), inferring a pH-triggered release pattern. The pH-sensitive releasing ability of DOX is remarkable, owing to tumor/cancer cells (pH 4–5) and tumor tissue (pH 6.8) are found in an acidic environment [59]. Thus, DOX loading could be released rapidly release in cancer cells and tissues.

The dissolution evaluation in Fig. S2 showed that the kinetics model resulted by FACDs-DOX at pH 5.5, 7.4, and 9.0 followed the Korsmeyer-Peppas kinetics model. This is based on the quantity of the R^2 value of the release test on pH 5.5, 7.4, and 9.0 medium is 0.97; 0.98; 0.98, respectively, which can be observed in Table S2. Moreover, the Chi-square value (χ^2) was used as a function of statistical error during the study [60]. The lowest Chi-square (χ^2) value indicates the best-fitted model of drug release kinetics [61]. According to Table S2, the lowest value of χ^2 was found in the Korsmeyer-Peppas kinetics model, with χ^2 release test on pH 5.5, 7.4, and 9.0 medium signifying 6.876296; 6.320155; and 1.800886, respectively. Contrasting with the Higuchi model, which explains the drug release from the common drug matrix, the Korsmeyer-Peppas model is formed of drug release particularly from a polymeric system, where the drug needs to overwhelm the polymer interference through the process of release [62]. Moreover, DOX release follows Fickian diffusion due to the n value of Korsmeyer-Peppas of all FACDs-DOX are under 0.5. This is verified based on the DOX release formation of concentration gradients. Furthermore, pH greatly affects the release rate of DOX which can be observed from the K value of each FACDs-DOX. The *k* FACDs-DOX values (pH 5.5, 7.4, 9.0) were 1.731988, 1.482661, and 0.371576, respectively. From these data, there are major interaction of DOX and carbon dots by hydrogen bonding (-OH···O and –CH···O-) and also van der Waals interactions. According to the previous study, the protonation of the amine group ($-NH_2$) was higher in an acidic environment (pH 6.4) that supported the process of diffusion toward higher solubility. Surprisingly, the extracellular pH of tumor cells is acidic (~6.5–6.9) that could be more favorable for cancer therapy [63].

3.2. In vitro assessments

CCK-8 assay was applied to assess the cytotoxicity of the FACDs by using HeLa cells. The varying concentrations of FACDs are from 0 to 400 mg/mL for 24 h. The cell viability was noticed from Fig. 7, which were perceived that the cells survival rates were above 80% even though the concentration is up to 500 μg mL^{-1}. Furthermore, the CC_{50} value of FACDs-P2 in Fig. S3 showed a high concentration up to 71878.14 μg mL^{-1}. It confirmed that the FACDs were non-toxic and great biocompatible with HeLa cells, which could be a potential agent in the field of bioimaging application [64]. The CLSM of the FACDs shown in Fig. 8 for fluorescence imaging of cancer cells is dependent on the extent of folate receptor expression in HeLa cancer cells. HeLa cells exhibit specific characteristics owing to their surface is abundant in folate receptors [8,

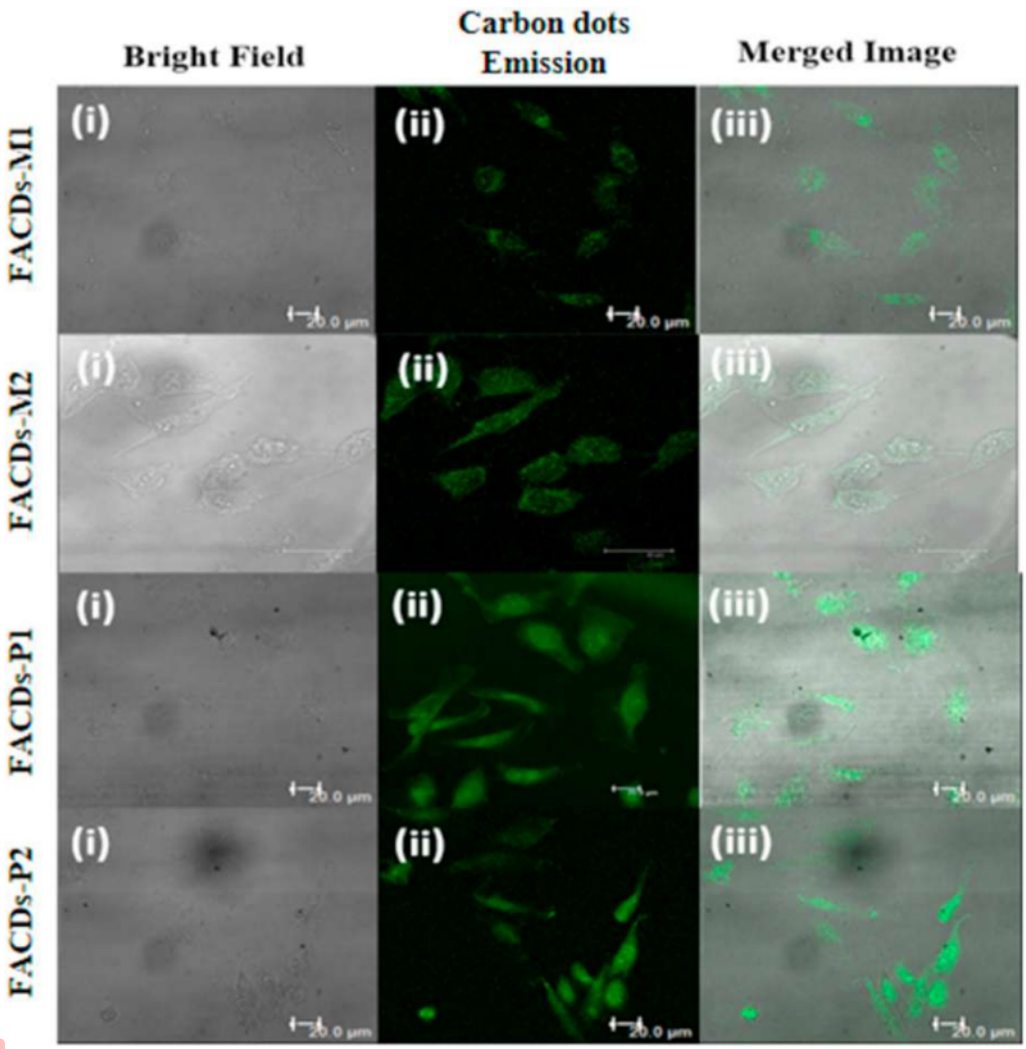

Fig. 8. Photograph CLSM images of HeLa cells after 1 h incubated with folic acid-based carbon dots by excitation at 488 nm. The scale bars represent 20 μm.

65]. Moreover, Confocal Laser Scanning Microscopy (CLSM) data demonstrated the outstanding cell selectivity of FACDs as well as consistency in surface binding and absorption of FACDs by cells. The results indicated that the FA sites on CDs could facilitate intracellular folic acid uptake via receptor-mediated endocytosis. Endocytosis is a common mechanism by which various extracellular materials that internalized into cells as shown in Scheme 2. Furthermore, the Z stacking mode in CLSM was also used in proving FACDs in the cell cytoplasm. From the data in Fig. S4, the accumulation of FACDs in cells constitutes an active targeting package as well as an endocytosis process to make them exist in the cell cytoplasm.

Further in vitro analysis involved doping CDs on HeLa cells by measuring flow cytometry. Flow cytometry tests are performed to quantify and identify the fluorescence of accumulated material toward HeLa cells. Annexin V-FITC and propidium iodide (PI) were both applied for cell staining. In phosphatidylserine, high affinity is shown by Annexin V-FITC which can be transferred to the outward layer of the cell membrane within the apoptosis process. The cell necrosis can be identified by PI (flow cytometry kit) through RNA and DNA interaction in the cells [66]. For the controlled group (untreated HeLa cell) in Fig. 9, the live cells identified in nearly 100%. Otherwise, the cells which co-incubated by FACDs-P1, FACDs-P2, FACDs-M1, and FACDs-2 were slightly decreased to 98.26%, 93.05%, 97.25%, and 93.1%, respectively. Furthermore, all FACDs showed early apoptosis under 3.50%, which indicated the low toxicity of each FACDs in the HeLa cell and proof the CCK-8 assay measurement. In contrast, the FACDs-P1/DOX percentage of the cells dramatically declined to 43.33%, whereas the early and late apoptosis cells dramatically raised to 27.56% and 16.22%, respectively. Apoptosis is a phenomenon in which cells die due to external interference, in this case, DOX, which destroys the DNA conformation in the cell [18]. Therefore, the FACDs-P1/DOX can strongly detect HeLa cells, deliver drugs, and destroy the targeted cancer cells.

4. Conclusion

As result, Carbon dots can be fabricated from folic acid-based by the process of a furnace and microwave-assisted carbonization. Some characterizations confirmed the successful FACDs with the highest

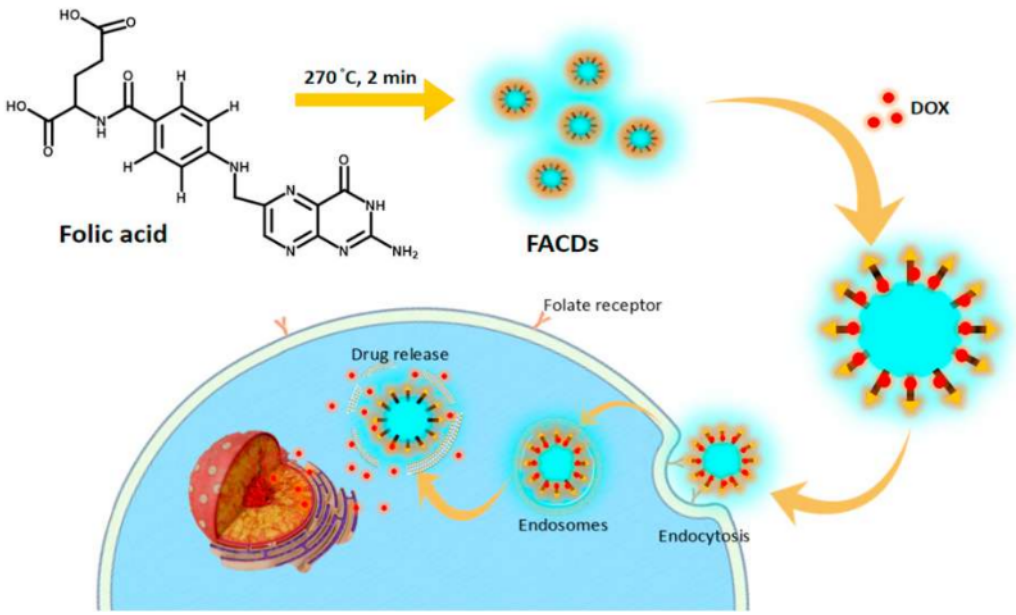

Scheme 2. Internalization schematic route of the FACDs–DOX conjugate into a HeLa cell lines.

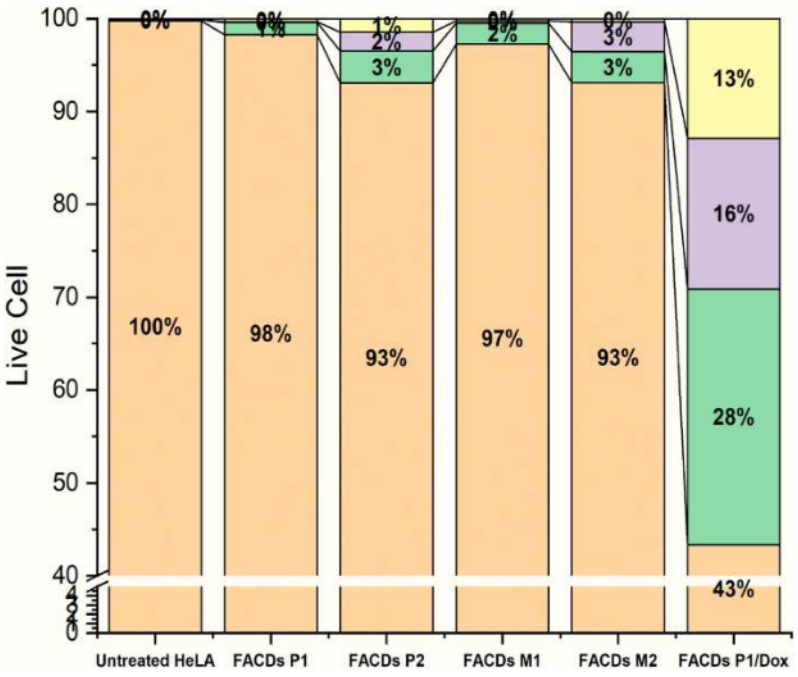

Fig. 9. The histogram representing the flow cytometry data of each FACDs; live cell (LT orange); early apoptosis (LT green); late apoptosis (LT purple); early necrosis (LT yellow). (For interpretation of the references to colour in this figure legend, the reader is referred to the Web version of this article.)

optical property (QY value 55.7%), the cytotoxicity evaluation unveils that all FACDs are non-toxic. CLSM study increased the potency application of FACDs as bioimaging agents. Distinctly, the DOX release rate was higher in the acidic pH state than in the neutral or basic state, due to protonation that was initiated by hydrogen bonding and van der Waals interactions. The DOX release of the CDs matches the Korsmeyer-Peppas kinetic model.

CRediT authorship contribution statement

Mochamad Z. Fahmi: Conceptualization, Writing – review & editing, Supervision. **Novia F. Sholihah:** Investigation. **Aswandi Wibrianto:** Investigation. **Satya C.W. Sakti:** Validation. **Fakhri Firdaus:** Investigation. **Jia-yaw Chang:** Validation, Supervision.

Declaration of competing interest

The authors declare that they have no known competing financial interests or personal relationships that could have appeared to influence the work reported in this paper.

Acknowledgments

The authors thank the Ministry of Research and Technology Republic of Indonesia for research support under contract No. 808/UN3.14/LT/2020 and Universitas Airlangga for Research Facilities.

Appendix A. Supplementary data

Supplementary data to this article can be found online at https://doi.org/10.1016/j.matchemphys.2021.124596.

References

[1] N. Kuplennik, K. Lang, R. Steinfeld, A. Sosnik, Folate receptor α-modified nanoparticles for targeting of the central nervous system, ACS Appl. Mater. Interfaces 11 (2019) 39633–39647.
[2] M.Z. Fahmi, J.-Y. Chang, A facile strategy to enable nanoparticles for simultaneous phase transfer, folate receptor targeting, and cisplatin delivery, RSC Adv. 4 (2014) 56713–56721.
[3] Y. Liu, P. Wu, X. Wu, C. Ma, S. Luo, M. Xu, et al., Nitrogen and copper (II) co-doped carbon dots for applications in ascorbic acid determination by non-oxidation reduction strategy and cellular imaging, Talanta 210 (2020) 120649.
[4] P.-H. Wu, A.E. Opadele, Y. Onodera, J.-M. Nam, Targeting integrins in cancer nanomedicine: applications in cancer diagnosis and therapy, Cancers 11 (2019) 1783.
[5] M.R. Sepand, M. Ghavami, S. Zanganeh, S. Stacks, F. Ghasemi, H. Montazeri, et al., Impact of plasma concentration of transferrin on targeting capacity of nanoparticles, Nanoscale 12 (2020) 4935–4944.
[6] Y. Wang, Z. Jiang, B. Yuan, Y. Tian, L. Xiang, Y. Li, et al., AY 1 receptor ligand synergized with a P-glycoprotein inhibitor improves the therapeutic efficacy of multidrug resistant breast cancer, Biomaterials science 7 (2019) 4748–4757.
[7] M. Satpathy, L. Wang, R.J. Zielinski, W. Qian, Y.A. Wang, A.M. Mohs, et al., Targeted drug delivery and image-guided therapy of heterogeneous ovarian cancer using her2-targeted theranostic nanoparticles, Theranostics 9 (2019) 778.
[8] H. Liu, Z. Li, Y. Sun, X. Geng, Y. Hu, H. Meng, et al., Synthesis of luminescent carbon dots with ultrahigh quantum yield and inherent folate receptor-positive cancer cell targetability, Sci. Rep. 8 (2018) 1–8.
[9] K.R. Bittleman, S. Dong, M. Roman, Y.W. Lee, Folic acid-conjugated cellulose nanocrystals show high folate-receptor binding affinity and uptake by KB and breast cancer cells, ACS Omega 3 (2018) 13952–13959.
[10] M.-Y. Fei, M.-M. Song, P. Wang, G-z Pang, J. Chen, D.-P. Lu, et al., Folic acid modified Fe_3O_4 nanoclusters by a one-step ultrasonic technique for drug delivery and MR imaging, RSC Adv. 10 (2020) 5294–5303.
[11] S. Raniolo, G. Vindigni, V. Unida, A. Ottaviani, E. Romano, A. Desideri, et al., Entry, fate and degradation of DNA nanocages in mammalian cells: a matter of receptors, Nanoscale 10 (2018) 12078–12086.
[12] X. Zhao, J. Zhang, L. Shi, M. Xian, C. Dong, S. Shuang, Folic acid-conjugated carbon dots as green fluorescent probes based on cellular targeting imaging for recognizing cancer cells, RSC Adv. 7 (2017) 42159–42167.
[13] A. Mewada, S. Pandey, M. Thakur, D. Jadhav, M. Sharon, Swarming carbon dots for folic acid mediated delivery of doxorubicin and biological imaging, J. Mater. Chem. B 2 (2014) 698–705.
[14] S. Li, J. Jiang, Y. Yan, P. Wang, G. Huang, N. hoon Kim, et al., Red, green, and blue fluorescent folate-receptor-targeting carbon dots for cervical cancer cellular and tissue imaging, Mater. Sci. Eng. C 93 (2018) 1054–1063.
[15] S.K. Bhunia, A.R. Maity, S. Nandi, D. Stepensky, R. Jelinek, Imaging cancer cells expressing the folate receptor with carbon dots produced from folic acid, Chembiochem 17 (2016) 614–619.
[16] T.S. Atabaev, Doped carbon dots for sensing and bioimaging applications: a minireview, Nanomaterials 8 (2018) 342.
[17] L. Thoo, M.Z. Fahmi, I.N. Zulkipli, N. Keasberry, A. Idris, Interaction and cellular uptake of surface-modified carbon dot nanoparticles by J774. 1 macrophages, Cent. Eur. J. Immunol. 42 (2017) 324.
[18] M.Z. Fahmi, A. Haris, A.J. Permana, D.L. Nor Wibowo, B. Purwanto, Y.L. Nikmah, et al., Bamboo leaf-based carbon dots for efficient tumor imaging and therapy, RSC Adv. 8 (2018) 38376–38383.
[19] Z.L. Wu, Z.X. Liu, Y.H. Yuan, Carbon dots: materials, synthesis, properties and approaches to long-wavelength and multicolor emission, J. Mater. Chem. B 5 (2017) 3794–3809.
[20] N. Sano, T. Suntornlohanakul, C. Poonjarernsilp, H. Tamon, T. Charinpanitkul, Controlled syntheses of various palladium alloy nanoparticles dispersed in single-walled carbon nanohorns by one-step formation using an arc discharge method, Ind. Eng. Chem. Res. 53 (2014) 4732–4738.
[21] H.P. Castro, V.S. Souza, J.D. Scholten, J.H. Dias, J.A. Fernandes, F.S. Rodembusch, et al., Synthesis and characterisation of fluorescent carbon nanodots produced in ionic liquids by laser ablation, Chemistry–A European Journal 22 (2016) 138–143.
[22] A. Alam, C. Wan, T. McNally, Surface amination of carbon nanoparticles for modification of epoxy resins: plasma-treatment vs. wet-chemistry approach, Eur. Polym. J. 87 (2017) 422–448.
[23] Y.-Y. Yao, G. Gedda, W.M. Girma, C.-L. Yen, Y.-C. Ling, J.-Y. Chang, Magnetofluorescent carbon dots derived from crab shell for targeted dual-modality bioimaging and drug delivery, ACS Appl. Mater. Interfaces 9 (2017) 13887–13899.
[24] M. Semeniuk, Z. Yi, V. Poursorkhabi, J. Tjong, S. Jaffer, Z.-H. Lu, et al., Future perspectives and review on organic carbon dots in electronic applications, ACS Nano 13 (2019) 6224–6255.
[25] T.V. de Medeiros, J. Manioudakis, F. Noun, J.-R. Macairan, F. Victoria, R. Naccache, Microwave-assisted synthesis of carbon dots and their applications, J. Mater. Chem. C 7 (2019) 7175–7195.
[26] Y. Zheng, D. Yang, X. Wu, H. Yan, Y. Zhao, B. Feng, et al., A facile approach for the synthesis of highly luminescent carbon dots using vitamin-based small organic molecules with benzene ring structure as precursors, RSC Adv. 5 (2015) 90245–90254.
[27] V.S. Sivasankarapillai, A.V. Kirthi, M. Akksadha, S. Indu, U.D. Dharshini, J. Pushpamalar, et al., Recent advancements in the applications of carbon nanodots: exploring the rising star of nanotechnology, Nanoscale Advances 2 (2020) 1760–1773.
[28] P. Koutsogiannis, E. Thomou, H. Stamatis, D. Gournis, P. Rudolf, Advances in fluorescent carbon dots for biomedical applications, Adv. Phys. X 5 (2020), 1758592.
[29] A. Wibrianto, S.Q. Khairunisa, S.C. Sakti, Y.L. Ni'mah, B. Purwanto, M.Z. Fahmi, Comparison of the effects of synthesis methods of B, N, S, and P-doped carbon dots with high photoluminescence properties on HeLa tumor cells, RSC Adv. 11 (2021) 1098–1108.
[30] M.Z. Fahmi, W. Sukmayani, S.Q. Khairunisa, A.M. Witaningrum, D.W. Indriati, M. Q.Y. Matondang, et al., Design of boronic acid-attributed carbon dots on inhibits HIV-1 entry, RSC Adv. 6 (2016) 92996–93002.
[31] W. Liu, C. Li, Y. Ren, X. Sun, W. Pan, Y. Li, et al., Carbon dots: surface engineering and applications, J. Mater. Chem. B 4 (2016) 5772–5788.
[32] Z. Zhang, Y. Lei, X. Yang, N. Shi, L. Geng, S. Wang, et al., High drug-loading system of hollow carbon dots–doxorubicin: preparation, in vitro release and pH-targeted research, J. Mater. Chem. B 7 (2019) 2130–2137.
[33] S. Kalytchuk, L. Zdražil, M. Scheibe, R. Zbořil, Purple-emissive carbon dots enhance sensitivity of Si photodetectors to ultraviolet range, Nanoscale 12 (2020) 8379–8384.
[34] J. Zhang, X. Zhao, M. Xian, C. Dong, S. Shuang, Folic acid-conjugated green luminescent carbon dots as a nanoprobe for identifying folate receptor-positive cancer cells, Talanta 183 (2018) 39–47.
[35] T. Deng, R. Zhang, J. Wang, X. Song, F. Bao, Y. Gu, et al., Carbon dots-cluster-DOX nanocomposites fabricated by a Co-Self-Assembly strategy for tumor-targeted bioimaging and therapy, Part. Part. Syst. Char. 35 (2018), 1800190.
[36] Y. Dong, P. Du, P. Liu, Absolutely "off–on" fluorescent CD-based nanotheranostics for tumor intracellular real-time imaging and pH-triggered DOX delivery, J. Mater. Chem. B 8 (2020) 8002–8009.
[37] E. Roduner, Size matters: why nanomaterials are different, Chem. Soc. Rev. 35 (2006) 583–592.
[38] T. Feng, Q. Zeng, S. Lu, X. Yan, J. Liu, S. Tao, et al., Color-tunable carbon dots possessing solid-state emission for full-color light-emitting diodes applications, ACS Photonics 5 (2018) 502–510.
[39] C.M. Carbonaro, R. Corpino, M. Salis, F. Mocci, S.V. Thakkar, C. Olla, et al., On the emission properties of carbon dots: reviewing data and discussing models, C—Journal of Carbon Research 5 (2019) 60.
[40] D. Tong, W. Li, Y. Zhao, L. Zhang, J. Zheng, T. Cai, et al., Non-conjugated polyurethane polymer dots based on crosslink enhanced emission (CEE) and application in Fe 3+ sensing, RSC Adv. 6 (2016) 97137–97141.
[41] Z. Feng, G. Wu, C. Liu, D. Li, B. Jiang, X. Zhang, Edible coating based on whey protein isolate nanofibrils for antioxidation and inhibition of product browning, Food Hydrocolloids 79 (2018) 179–188.
[42] K. Kumar, S. Kaur, S. Kaur, G. Bhargava, S. Kumar, P. Singh, Self-assembled nanofibers of perylene diimide for the detection of hypochlorite in water, bio-fluids and solid-state: exogenous and endogenous bioimaging of hypochlorite in cells, J. Mater. Chem. B 8 (2020) 125–135.

[43] X. Lin, Y. Cao, J. Li, D. Zheng, S. Lan, Y. Xue, et al., Folic acid-modified Prussian blue/polydopamine nanoparticles as an MRI agent for use in targeted chemo/photothermal therapy, Biomaterials science 7 (2019) 2996–3006.
[44] P. Manivasagan, S.W. Jun, N.T.P. Truong, G. Hoang, S. Mondal, M.S. Moorthy, et al., A multifunctional near-infrared laser-triggered drug delivery system using folic acid conjugated chitosan oligosaccharide encapsulated gold nanorods for targeted chemo-photothermal therapy, J. Mater. Chem. B 7 (2019) 3811–3825.
[45] M.L. Desai, S. Jha, H. Basu, R.K. Singhal, P. Sharma, S.K. Kailasa, Microwave-assisted synthesis of water-soluble Eu 3+ hybrid carbon dots with enhanced fluorescence for the sensing of Hg 2+ ions and imaging of fungal cells, New J. Chem. 42 (2018) 6125–6133.
[46] M. Tuerhong, X. Yang, Y. Xue-bo, Review on carbon dots and their applications, Chin. J. Anal. Chem. 45 (2017) 139–150.
[47] S. Bhattacharya, R.S. Phatake, S. Nabha Barnea, N. Zerby, J.-J. Zhu, R. Shikler, et al., Fluorescent self-healing carbon dot/polymer gels, ACS Nano 13 (2019) 1433–1442.
[48] X. Sun, C. Bruckner, Y. Lei, One-pot and ultrafast synthesis of nitrogen and phosphorus co- doped carbon dots possessing bright dual wavelength fluorescence emission, Nanoscale 7 (2013) 17278–17282.
[49] M. Zheng, L. Qiao, Y. Su, P. Gao, Z. Xie, A postmodification strategy to modulate the photoluminescence of carbon dots from blue to green and red: synthesis and applications, J. Mater. Chem. B 7 (2019) 3840–3845.
[50] D. Qu, M. Zheng, L. Zhang, H. Zhao, Z. Xie, X. Jing, et al., Formation mechanism and optimization of highly luminescent N-doped graphene quantum dots, Sci. Rep. 4 (2014) 1–11.
[51] J. Zhao, F. Li, S. Zhang, Y. An, S. Sun, Preparation of N-doped yellow carbon dots and N, P co-doped red carbon dots for bioimaging and photodynamic therapy of tumors, New J. Chem. 43 (2019) 6332–6342.
[52] K. Hola, M. Sudolska, S. Kalytchuk, D. Nachtigallova, A.L. Rogach, M. Otyepka, et al., Graphitic nitrogen triggers red fluorescence in carbon dots, ACS Nano 11 (2017) 12402–12410.
[53] V.B. Kumar, A.K. Sahu, A.S. Mohsin, X. Li, A. Gedanken, Refractive-index tuning of highly fluorescent carbon dots, ACS Appl. Mater. Interfaces 9 (2017) 28930–28938.
[54] W. Li, M. Li, Y. Liu, D. Pan, Z. Li, L. Wang, et al., Three minute ultrarapid microwave-assisted synthesis of bright fluorescent graphene quantum dots for live cell staining and white LEDs, ACS Applied Nano Materials 1 (2018) 1623–1630.
[55] R. Ravanshad, A.K. Zadeh, A.M. Amani, M. Mousavi, S.A. Hashemi, A.S. Dashtaki, et al., Application of nanoparticles in cancer detection by Raman scattering based techniques, Nano Reviews & Experiments 9 (2018), 1373551.
[56] S. Bhattacharyya, B. Konkena, K. Jayaramulu, W. Schuhmann, T.K. Maji, Synthesis of nano-porous carbon and nitrogen doped carbon dots from an anionic MOF: a trace cobalt metal residue in carbon dots promotes electrocatalytic ORR activity, J. Mater. Chem. 5 (2017) 13573–13580.
[57] Y. Zhou, Y. Sun, C. Zhu, Y. Liu, X. Dai, J. Zhong, et al., C–O^-–K^+(Na^+) groups in non-doped carbon as active sites for the oxygen reduction reaction, J. Mater. Chem. 6 (2018) 8955–8961.
[58] C.V.M. Gopi, S. Ravi, S.S. Rao, A.E. Reddy, H.-J. Kim, Carbon nanotube/metal-sulfide composite flexible electrodes for high-performance quantum dot-sensitized solar cells and supercapacitors, Sci. Rep. 7 (2017) 46519.
[59] P. Xu, H. Zuo, B. Chen, R. Wang, A. Ahmed, Y. Hu, et al., Doxorubicin-loaded platelets as a smart drug delivery system: an improved therapy for lymphoma, Sci. Rep. 7 (2017) 42632.
[60] G.R. Mahdavinia, H. Etemadi, In situ synthesis of magnetic CaraPVA IPN nanocomposite hydrogels and controlled drug release, Mater. Sci. Eng. C 45 (2014) 250–260.
[61] R. Osae, G. Essilfie, R.N. Alolga, E. Bonah, H. Ma, C. Zhou, Drying of ginger slices—evaluation of quality attributes, energy consumption, and kinetics study, J. Food Process. Eng. 43 (2020), e13348.
[62] M.Z. Fahmi, R.A. Prasetya, M.F. Dzikri, S.C.W. Sakti, B. Yuliarto, $MnFe_2O_4$ nanoparticles/cellulose acetate composite nanofiber for controllable release of naproxen, Mater. Chem. Phys. 250 (2020), 123055.
[63] S. Salimi, R. Sotudeh-Gharebagh, R. Zarghami, S.Y. Chan, K.H. Yuen, Production of nanocellulose and its applications in drug delivery: a critical review, ACS Sustain. Chem. Eng. 7 (2019) 15800–15827.
[64] P. Shen, J. Gao, J. Cong, Z. Liu, C. Li, J. Yao, Synthesis of cellulose-based carbon dots for bioimaging, Chemistry 1 (2016) 1314–1317.
[65] K. Siwowska, R.M. Schmid, S. Cohrs, R. Schibli, C. Müller, Folate receptor-positive gynecological cancer cells: in vitro and in vivo characterization, Pharmaceuticals 10 (2017) 72.
[66] M.Z. Fahmi, K.-L. Ou, J.-K. Chen, M.-H. Ho, S.-H. Tzing, J.-Y. Chang, Development of bovine serum albumin-modified hybrid nanoclusters for magnetofluorescence imaging and drug delivery, RSC Adv. 4 (2014) 32762–32772.

Simple and fast design of folic acid-based carbon dots as theranostic agent and its drug release aspect

ORIGINALITY REPORT

10%	2%	13%	4%
SIMILARITY INDEX	INTERNET SOURCES	PUBLICATIONS	STUDENT PAPERS

PRIMARY SOURCES

1	Yu-Yu Aung, Aswandi Wibrianto, Jefry S. Sianturi, Desita K. Ulfa et al. "Comparison Direct Synthesis of Hyaluronic Acid-Based Carbon Nanodots as Dual Active Targeting and Imaging of HeLa Cancer Cells", ACS Omega, 2021 Publication	3%
2	Mochamad Zakki Fahmi, Roch Adi Prasetya, Muhammad Fathan Dzikri, Satya Candra Wibawa Sakti et al. "MnFe2O4 nanoparticles/cellulose acetate composite nanofiber for controllable release of naproxen", Materials Chemistry and Physics, 2020 Publication	2%
3	Fahmi, Mochamad Zakki, Jem-Kun Chen, Chih-Ching Huang, Yong-Chien Ling, and Jia-Yaw Chang. "Phenylboronic acid-modified magnetic nanoparticles as a platform for carbon dot conjugation and doxorubicin	1%

delivery", Journal of Materials Chemistry B, 2015.
Publication

4	Fahmi, A.. "Aggregation of oligothio dendrimer-semi-capped nanoparticles on solid surfaces: Droplets and 'doughnuts'", Materials Chemistry & Physics, 20070615 Publication	1 %
5	Mochamad Zakki Fahmi, Abdul Haris, Ahmadi Jaya Permana, Denika Liyan Nor Wibowo et al. "Bamboo leaf-based carbon dots for efficient tumor imaging and therapy", RSC Advances, 2018 Publication	1 %
6	Anu Babusenan, B. Pandey, Somnath C. Roy, Jayeeta Bhattacharyya. "Charge transfer mediated photoluminescence enhancement in carbon dots embedded in TiO2 nanotube matrix", Carbon, 2020 Publication	1 %
7	Mochamad Zakki Fahmi, Keng-Liang Ou, Jem-Kun Chen, Ming-Hua Ho, Shin-Hwa Tzing, Jia-Yaw Chang. "Development of bovine serum albumin-modified hybrid nanoclusters for magnetofluorescence imaging and drug delivery", RSC Adv., 2014 Publication	1 %

8	"Prelim III: Contents", Materials Chemistry and Physics, 2021 Publication	1 %
9	Bhunia, Susanta, Amit Maity, Sukhendu Nandi, David Stepensky, and Raz Jelinek. "Imaging cancer cells expressing the folate receptor with carbon dots produced from folic acid", ChemBioChem, 2016. Publication	1 %

Exclude quotes	On	Exclude matches	< 1%
Exclude bibliography	On		

Simple and fast design of folic acid-based carbon dots as theranostic agent and its drug release aspect

GRADEMARK REPORT

FINAL GRADE

/0

GENERAL COMMENTS

Instructor

PAGE 1

PAGE 2

PAGE 3

PAGE 4

PAGE 5

PAGE 6

PAGE 7

PAGE 8

PAGE 9

PAGE 10

PAGE 11